Makara Journal of Science

Volume 26
Issue 3 *September*

Article 6

9-30-2022

Comparative Photovoltaics of P3HT:N2200 and P3HT: Small-Gap Fullerene Ethyl-Nipecotate Bulk Heterojunction Structures

Md. Nasir Uddin
Department of Physics, Mawlana Bhashani Science and Technology University, Tangail 1902, Bangladesh, mnuraju@gmail.com

Rafiqul Islam
Department of Electrical and Electronic Engineering, Leading University, Sylhet 3112, Bangladesh

Muhibur Rahman
Department of Physics, Shahjalal University of Science and Technology, Sylhet 3114, Bangladesh

Nazia Chawdhury
Department of Physics, Shahjalal University of Science and Technology, Sylhet 3114, Bangladesh

Makara Journal of Science, 26/3 (2022), 200–208
doi: 10.7454/mss.v26i3.1370

Comparative Photovoltaics of P3HT:N2200 and P3HT: Small-Gap Fullerene Ethyl-Nipecotate Bulk Heterojunction Structures

Md. Nasir Uddin[1*], Rafiqul Islam[2], Muhibur Rahman[3], and Nazia Chawdhury[3]

1. Department of Physics, Mawlana Bhashani Science and Technology University, Tangail 1902, Bangladesh
2. Department of Electrical and Electronic Engineering, Leading University, Sylhet 3112, Bangladesh
3. Department of Physics, Shahjalal University of Science and Technology, Sylhet 3114, Bangladesh

[*]*E-mail: nasiruddin@mbstu.ac.bd*

Received June 23, 202 | Accepted September 16, 2022

Abstract

This work deals with the study on the optical absorption and photoluminescence spectra of a p-type organic semiconducting polymer, regioregular poly 3-hexylthiophene-2,5-diyl (P3HT) and the absorption spectra of an n-type fullerene-based small-gap fullerene-ethyl nipecotate (Fullerene-EN) and a non-fullerene-based polynaphthalene bithiophene (N2200) semiconducting materials. The band gap of P3HT, N2200, and small-gap fullerene-ethyl nipecotate are 2.42, 1.65, and 1.51 eV, respectively, calculated from experimental results through the Tauc equation. Active layers with blends of P3HT and small-gap fullerene-ethyl nipecotate and P3HT and N2200 have been used to fabricate bulk heterojunction (BHJ) structures. The P3HT:N2200 BHJ structure follows the current density versus voltage characteristics of a photovoltaic device with 0.28% power conversion efficiency, 1.58 mA/cm^2 short-circuit current density, and 41% fill factor. However, the P3HT:small-gap fullerene-ethyl nipecotate structure does not show any photovoltaic *J–V* characteristics.

Keywords: bulk heterojunction, buffer layer, organic solar cell, photocurrent

Introduction

Organic materials have become very popular in the field of organic electronics since the discovery of conducting polyacetylene around November 1976. The conductivities in π-conjugated (hydrocarbon chains with alternate single and double bonds) organic semiconducting materials can be regulated by doping. Alan J. Heeger, Alan MacDiarmid, and Hideki Shirakawa were awarded with the Nobel Prize in Chemistry in 2000 for their discovery and development of these semiconducting polymers [1, 2]. Organic conjugated materials are also known as organic semiconducting materials because of their delocalized π-molecular orbitals. These π electrons are responsible for the semiconducting properties of these polymers. Due to their efficient charge transport and improved electroluminescent properties, these materials have been successfully used in many organic and hybrid electronic devices, such as organic light-emitting diodes, organic photovoltaics (OPVs), and organic field-effect transistors. In the field of organic electronics, poly(3-hexylthiophene-2,5-diyl) (P3HT) and poly(9,9-dioctylfluorene-alt-benzothiadiazole) are used as p-type donor materials. However, small-gap fullerene-ethyl nipecotate, fullerene-based phenyl-C61-butyric acid methyl ester (PCBM), and non-fullerene-based polynaphthalene-bithiophene (N2200) are the n-type acceptor materials. The molecular and supramolecular structures, band-gap energy, and semiconducting properties of these organic materials have become fundamental subjects over the past years [3-5]. Recently, researchers have studied the N2200 polymer to build efficient photoactive layers in bulk heterojunction (BHJ) solar cells with different donor polymers [6-9]. However, the literature reports that the electron mobility in solar cell devices increases with the use of the N2200 polymer as the donor along with fullerene derivatives as electron acceptor schemes [10]. Moreover, the maximum power conversion efficiency (PCE) exceeded 18% with the use of non-fullerene as acceptors in OPVs [11, 12].

The energy difference between the lower edge of the conduction band and the upper edge of the valence band is known as the band gap or band-gap energy of the material. In the case of organic materials, the energy gap signifies the energy difference between the highest occupied molecular orbital (HOMO) and lowest unoccupied molecular orbital (LUMO). These HOMO and LUMO energy levels are influenced by the molecular alignment and packing of materials. The conduction properties of organic semiconductors depend on the energy gap. The energy gap of organic π-conjugated semiconductors depends on the electronic band structure, pressure, and temperature [13, 14]. The band gap

calculation is very important for determining the electrical conductivity of solids and is extremely important in organic electronics to fabricate organic devices. The PCEs of photovoltaic cells fabricated with pure conjugated organic polymers are typically 10^{-3}%–10^{-2}% [15-17], which are too low to be used in solar cell applications. The discovery of photo-induced electron transfer in the combinations of conducting polymers as donors (p-type) and buckminsterfullerene (C_{60}) and its derivatives as acceptors (n-type) offers a molecular approach to an efficient photovoltaic power conversion [18, 19]. In 1995, the concept of the BHJ was first introduced. The journey of organic polymers begun with the blend of the polymer:acceptor. The blend of poly(3-hexylthiophene-2, 5-diyl) (P3HT) with [6,6]-phenyl-C_{61} butyric acid methyl ester (PCBM) had been widely studied for polymer:fullerene photovoltaic since the introduction of the BHJ structure [20]. This is because of the larger interfacial area in the BHJ devices than in the planar heterojunction, which leads to a higher short circuit current (I_{sc}). The PCE of the solution-processed organic solar cells using polymer acceptors is 17% [21, 22], which is very close to the maximum PCE of organic solar cells based on non-fullerene acceptors [23–26].

P3HT and PCBM exhibit a PCE of approximately 11% and have become promising materials [18]. Efficient device performance in organic BHJ solar cells can be obtained by introducing appropriate contact electrodes [27–29]. Researchers have suggested that buffer layers with some important modifications in BHJ, such as tuning the work function of the electrodes, improving the selectivity toward holes or electrons, and improving device stability, may enhance the device performance [30]. For P3HT:PCBM-based BHJ solar cells, a thin film (~nm) of lithium fluoride (LiF) is used as a cathode buffer layer with an Al cathode contact. Bathocuproine (BCP), a high-band-gap material, is also used as a hole-blocking or electron-transporting cathode buffer layer with the cathode contact to enhance the device performance. These contact layers improve the solar cell device parameters, such as the short-circuit current density (J_{sc}), open-circuit voltage (V_{oc}), and overall *PCE* [31].

In this work, the optical absorption spectra and optical band gap of P3HT, N2200, and small-gap fullerene-ethyl nipecotate were experimentally investigated in a chloroform solvent using UV–vis absorption spectroscopy. The band gaps of these materials were calculated using the Tauc equation. We presented a schematic diagram of a solar cell device structure to visualize the working principle of a solar cell and fabricated two solar cell devices with the P3HT:N2200 and P3HT:small-gap fullerene-ethyl nipecotate BHJ structures. The current density vs. voltage (*J*–*V*) characteristics of the devices were observed. The results found that the short-circuit current and open-circuit voltage condition exists only for the P3HT:N2200 BHJ structure. Therefore, the solar cell device parameters for the P3HT:N2200 BHJ structure were evaluated.

Experimental

Materials and methods. Indium tin oxide (ITO)-coated glass substrates with 25 mm × 25 mm × 1.1 mm and 12–15 Ω/sq surface resistivity were purchased from Luminescence Technology, Corp., Taiwan. Regioregular P3HT (M_W ~ 50,000–1000,000 g/mol), small-gap fullerene-ethyl nipecotate (M_W ~ 2100 g/mol), and BCP (M_W ~ 360.45 g/mol) were purchased from Sigma-Aldrich and were used without any further modification. N2200 was used as received from Organic Optoelectronic Materials Laboratory, Department of Chemistry, Korea University. The hole injecting material poly(3,4-ethylenedioxythiophene) polystyrene sulfonate (PEDOT:PSS) and cathode materials LiF and aluminum wire (99.9999% purity) were used from Organic Electronics Laboratory, Indian Institute of Technology Guwahati (IITG), India. The chemical structure of the materials used in this research is shown in Figure 1.

UV–vis absorption and photoluminescence (PL) measurements were taken using a UV–vis spectrophotometer (Shimadzu, UV-1800 PC) and spectrofluorophotometer (Shimadzu RF-5301 PC), respectively. The thin film of PEDOT:PSS and blend polymer solution on the top of the ITO substrate were fabricated outside and inside the glovebox, respectively, using a Laurell and Spin 150 spin-coater. The *J*–*V* characteristics of the devices were characterized using a Keithley-2400 digital source meter with a Newport Oriel Sol3A solar simulator, connected to an air mass 1.5 G filter at Organic Electronics Laboratory at IITG. The bulk heterojunction solar cell device structures are presented in Figure 2.

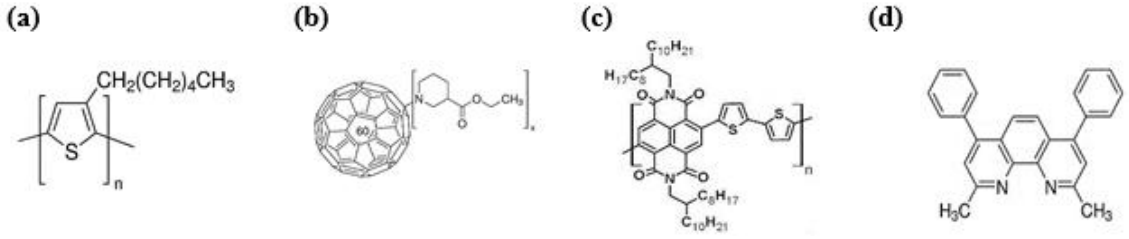

Figure 1. Schematic Representation of (a) P3HT, (b) Small-gap Fullerene-ethyl Nipecotate (Fullerene-EN), (c) N2200 Polymer, and (d) Bathocuproine

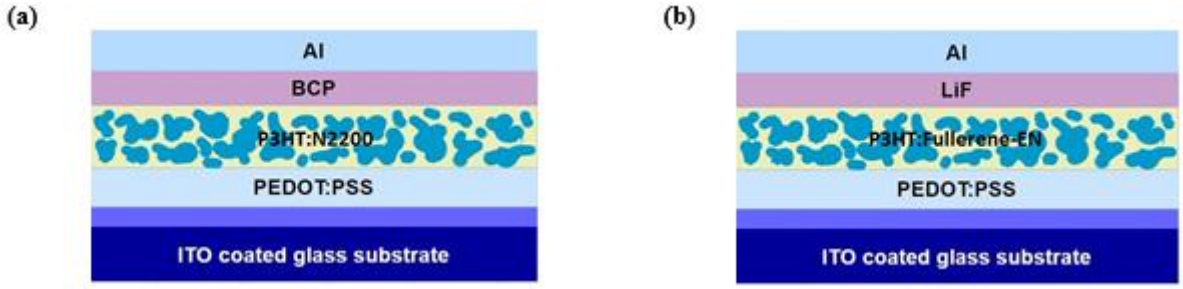

Figure 2. Schematic of the Fabricated (a) P3HT:N2200 and (b) P3HT:Fullerene-EN-based Bulk Heterojunction Organic Solar Cell

Sample preparation and device fabrication. For UV–vis absorption and PL spectra, 0.025 mg/ml of P3HT polymer solutions were prepared in a chloroform solvent at 26 ℃ temperature. In a similar way, individual solutions of N2200 and small-gap fullerene-ethyl nipecotate (Fullerene-EN) were prepared for the optical absorption study. The ITO-coated glass substrates were then sequentially cleaned in an ultrasonic cleaner in a soap solution, deionized water, acetone, and isopropanol solvent for a good fabrication. The substrates were dried under argon atmosphere, and then UV/ozone treatment was performed for approximately 20 min. Afterward, for PEDOT:PSS, the hole-injection buffer layer was spin-coated at 3000 rpm for 60 s on the top of ITO and dried at 120 ℃ for 30 min in an argon atmosphere. The blend of the P3HT:Fullerene-EN and P3HT:N2200 solutions with weight ratios of 1:0.6 and 1:1 was prepared in 1,2-dichlorobenzene (o-DCB) and chloroform solvent, respectively, and stirred for 48 h at 60 ℃ inside the glove box. The blend solutions were filtered with a 0.45μm PTFE filter and instantly spun over the PEDOT:PSS buffer layer. Approximately, 101 nm thin film of LiF/Al (LiF = 1 nm and Al = 100 nm) and ~108 nm thin film of BCP/Al (BCP = 8 nm and Al = 100 nm) cathode electrodes were thermally evaporated under a base pressure of ~10^{-6} mbar through a shadow mask. The active area of these fabricated devices was ~6 mm². The two structures of the fabricated devices are Device 1 (D1) and Device 2 (D2):

D1: ITO/PEDOT:PSS/P3HT:N2200 (1:1)/BCP/Al
D2: ITO/PEDOT:PSS/P3HT:Fullerene-EN (1:0.6)/LiF/Al

Results and Discussions

UV−vis and PL analysis. Figure 3(a) shows the absorption spectra of the P3HT (donor polymer), Fullerene-EN (acceptor material), and N2200 (acceptor polymer) in the solution state as a function of energy (eV). There are two absorption peaks with energies of 2.76 and 4.65 eV at the visible and UV ranges, respectively, which are attributed to the π–π^* transition [32–35]. Singh *et al*. studied the UV–vis absorption spectrum of P3HT in a solution form [30]. They found an absorption peak at a wavelength of 455 nm or 2.73 eV, whereas Geng and his research team reported a maximum absorbance of the P3HT solution at a wavelength of 449 nm or 2.76 eV [36]. They reported that these absorption peaks are due to the electronic transition from the HOMO to the LUMO of the P3HT polymer. A significant absorption was observed at the energy range of 1.5–5.0 eV for the N2200 solution. The absorption spectrum of N2200 showed two absorption regions with energies of 1.9 eV and 3.3 eV. The absorption peak at the lower energy (1.9 eV) is ascribed to the $S_0 \rightarrow S_1$ transition, which is mainly contributed by the HOMO→LUMO molecular orbital transition [37]. In addition, the absorbance maxima at an energy of 3.3 eV is characterized by the transition from the ground state (S_0) to different singlet excited states. Zhang *et al*. studied the UV–vis absorption spectrum of N2200 polymers [38]. They reported that the absorption spectrum of N2200 exhibits two absorption maxima at energies of 3.1 eV and 1.8 eV, which are attributed to the π–π^* and intramolecular charge transfer transitions, respectively. A similar work has been reported by Wen *et al*. in a chlorobenzene solution [37]. They reported that the absorption spectrum of N2200 exhibits two absorption maxima at energies of 3.18 eV and 1.77 eV. The absorption spectrum of Fullerene-EN did not show any distinct peak in the 1.5 eV–5.0 eV energy range, but it showed a rise from an energy of 1.5 eV–4.0 eV with a small bump at 4.5 eV and started to rapidly increase at higher energies. The onset of absorption signifies the band gap of the material, which is approximately 1.57 eV.

Figure 3(b) presents the normalized PL and absorption spectra of P3HT in the solution as a function of energy. The excitation wavelength for the PL spectrum was 450 nm (2.76 eV), where the absorption is maximum. A PL intensity peak was observed at energy of 2.18 eV. The maximum PL intensity corresponds to the onset of the HOMO–LUMO transition of the P3HT polymer [39]. In other words, the energy of the emitted photon is almost equal to the energy gap of the two states (HOMO and LUMO), which is the energy gap of the material. A red-shifted (0.57 eV) PL spectrum was also observed. This

finding confirmed that the energy of the emitted photon is lower than the absorbed energy by the P3HT polymer [40, 41]. Geng *et al*. also studied the PL spectrum of the P3HT solution with a maximum PL intensity at 568 nm or 2.18 eV [36].

Optical band gap calculation. According to the Beer–Lambert law; the intensity of the transmitted light is given by

$$I(l,\lambda) = I_0(\lambda)e^{-\alpha l}, \quad (1)$$

where $I_0(\lambda)$ is the intensity of incident light with wavelength λ, $I(l,\lambda)$ is the transmitted intensity of the light traveling the optical path length l.The band-gap energies of the materials were calculated using the value of the absorption coefficient α from the absorption spectra and Tauc plot method [42, 43]. Equation (1) turns into

$$\alpha = \frac{A}{l\log(e)} = 2.303\frac{A}{l}. \quad (2)$$

The optical path length of the cuvette used in this measurement was 1 cm, so the absorption coefficient is $\alpha = (2.303 \times A)$ cm^{-1}. Experimentally, "Tauc plot," also known as "Tauc gap," was used to calculate the band-gap energy of semiconductors with the Tauc equation [44, 45]

$$(\alpha h\nu)^n = K(h\nu - E_g), \quad (3)$$

where $h\nu$ is the photon energy, E_g is the band-gap energy, and *n* represents the nature of transitions [46]. The absorption coefficient $\alpha = (2.303 \times A)$ cm^{-1} with absorbance "*A*" is a function of energy. For direct, direct forbidden, indirect, and indirect forbidden transitions, the value of *n* is 2, $^2/_3$, $^1/_2$, and $^1/_3$, respectively [47, 48]. *K* is the energy independent coefficient, called a material constant. To determine the optical band-gap energy, $(\alpha h\nu)^n$ is plotted against $h\nu$ obtained from the UV–vis absorption spectra. The extrapolation of the linear part of the graph to the abscissa determines the band-gap energy of the semiconducting materials.

Figure 4(a) and 4(b) present the Tauc plot of $(\alpha h\nu)^2$ versus photon energy ($h\nu$) for P3HT and N2200. Figure 4(c) is the Tauc plot of $(\alpha h\nu)^{1/2}$ versus photon energy ($h\nu$) for the small-gap fullerene-ethyl nipecotate. The band gap of P3HT, N2200, and Fullerene-EN were 2.42, 1.65, and 1.51 eV, respectively, at 26 ℃ room temperature. Prasad *et al*. [49] and Anefnaf *et al*. [50] individually studied the UV–vis absorption spectroscopy of the P3HT thin film using chloroform and chlorobenzene solvents, respectively, and calculated the band gap of the P3HT film with 2.14 eV and 2.10 eV energies, respectively, using the Tauc equation. Gau *et al*. studied the UV–vis absorption spectra of N2200 in the solution and thin film [51]. They found a similar absorption profile for the solution and thin film state with a band-gap energy of 1.46 eV for the N2200 polymer. Similar results were obtained by Park *et al*. [52]. They reported that the band-gap energy of the N2200 polymer is 1.47 eV. Similarly, band-gap energy of 1.6 eV of the N2200 polymer was reported by Shinzaburo [53], where the absorption profile of this polymer is in good agreement to our experimental finding.

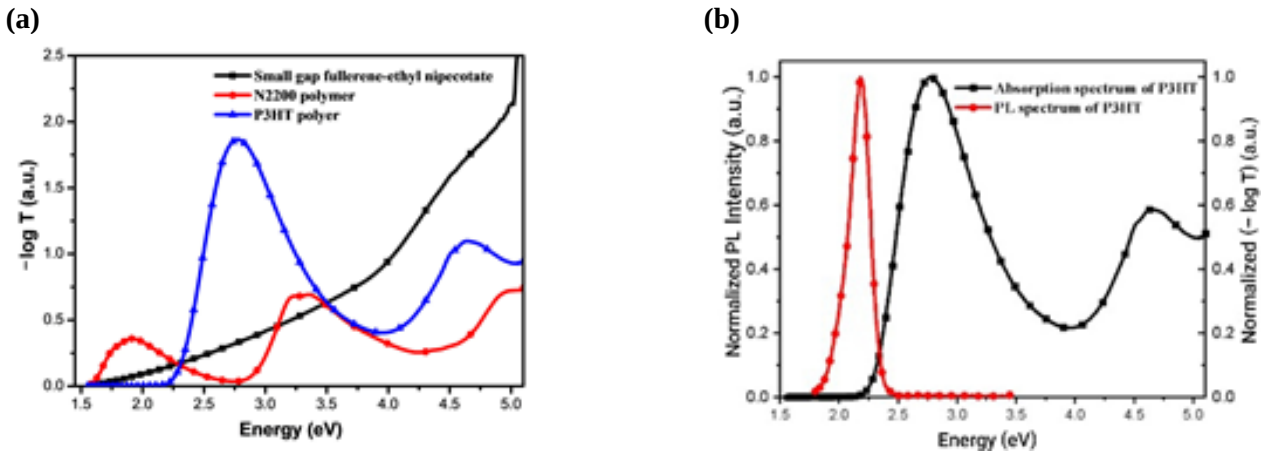

Figure 3. (a) UV–vis Absorption Spectra of P3HT (Blue Line), Fullerene-EN (Black Line), and N2200 (Red Line); (b) Normalized UV–vis Absorption and Photoluminescence Spectra of the P3HT Donor Polymer

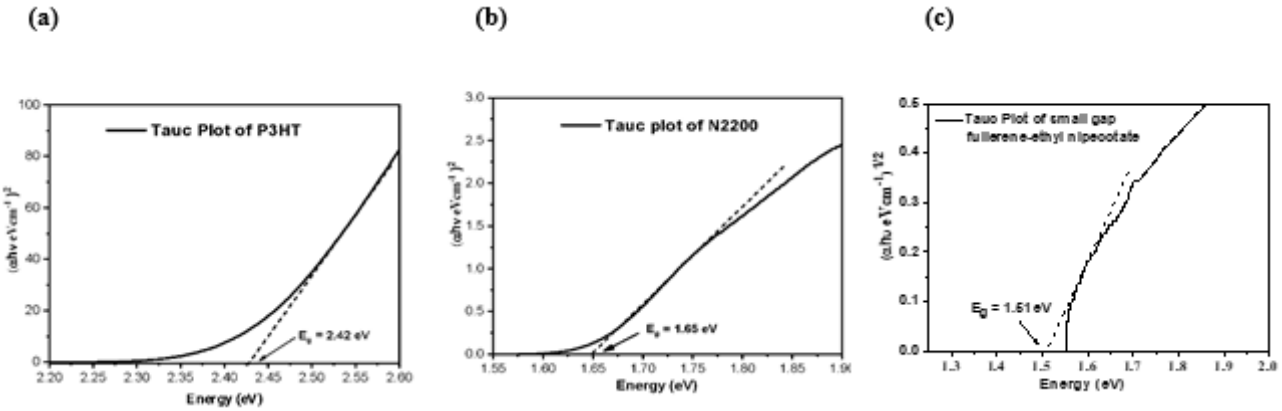

Figure 4. Tauc Plot for the Band Gap Calculation of (a) P3HT, (b) N2200, and (c) Fullerene-EN

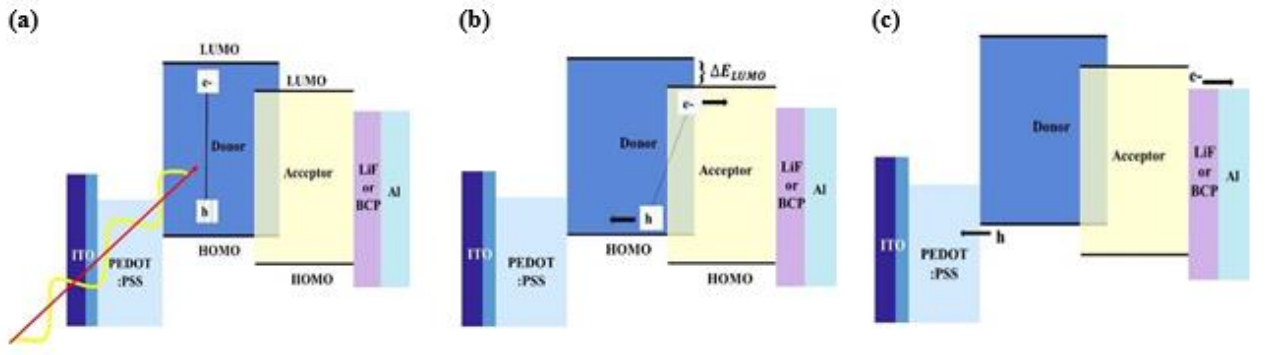

Figure 5. Schematic Diagram of the Organic Photovoltaic Operations for the Photocurrent Generation: (a) Exciton Generation, (b) Exciton Dissociation Into Free Carriers, and (c) Carrier Transport and Extraction

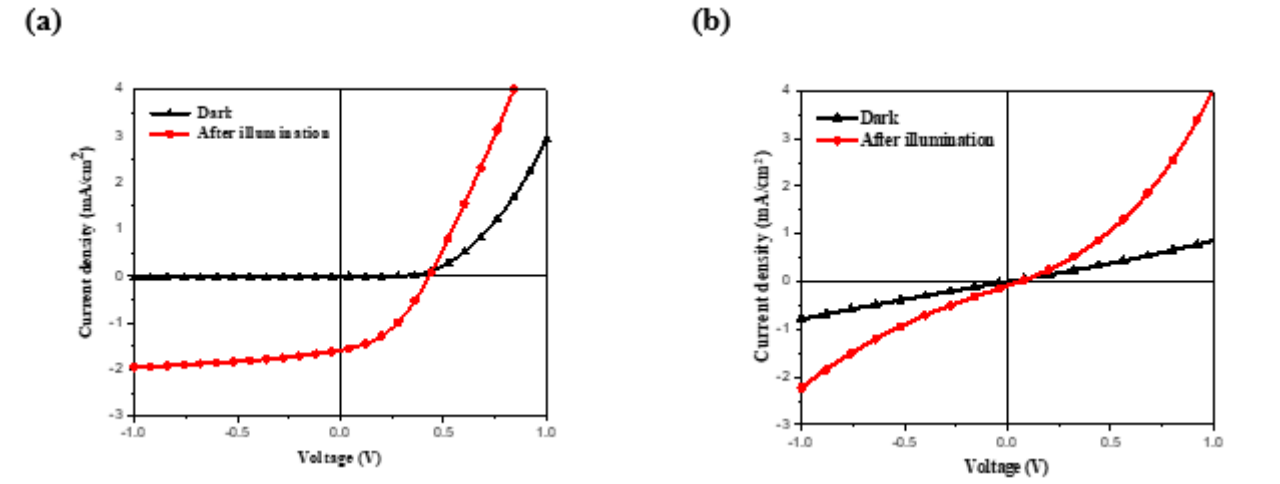

Figure 6. Current Density Versus Voltage *(J–V)* Characteristics of (a) ITO/PEDOT:PSS/P3HT:N2200 (1:1)/BCP/Al and (b) ITO/PEDOT:PSS/P3HT:Fullerene-EN (1:0.6)/LiF/Al

Photovoltaic characterization. Figure 5 illustrates the general photovoltaic device operation of an organic solar cell. The behavior of a solar cell device is identical to that of normal diodes under no-illumination condition or dark condition [54]. Therefore, the *J–V* curve of the solar cell device follows the *J–V* characteristics of normal diodes before illumination. Figure 6 displays the *J–V* characteristics of the P3HT:Fullerene-EN and P3HT:N2200 solution-based BHJ organic solar cell with weight ratios of 1:0.6 and 1:1, introduced with LiF/Al and BCP/Al cathode contacts, respectively. In the dark condition, D1 follows the *J–V* characteristics of a normal diode when the

external voltage is applied, as shown in Figure 6(a). However, in Figure 6(b), the curve does not follow such characteristics in the case of D2. The *J–V* curve in the dark condition became a straight line. This is because the fabricated BHJ structure with P3HT:Fullerene-EN is not so suitable for photovoltaic operations. The device behaves like ohmic material. After the illumination of light from the solar simulator, the current flow exponentially increased for D1 only. By contrast, a few amount of photocurrent increased for D2. This result is because the photo-generated exciton into the P3HT and Fullerene-EN interfaces did not efficiently dissociate to generate free charges. However, an efficient photoabsorption occurred in the P3HT polymer to generate photo excitons. The excited electrons returned toward the ground state for recombination. Efficient exciton dissociation will occur if the energy difference between E_{LUMO} of P3HT and E_{LUMO} of Fullerene-EN is greater than the exciton binding energy [55]. For an efficient exciton dissociation, the required donor–acceptor interface energy optimization condition is given by [18, 56-58]

$$\Delta E_{LUMO} = E_{LUMO}(donor) - E_{LUMO}(acceptor) > E_{Exciton}, \quad (4)$$

where $E_{Exciton}$ is the exciton binding energy.

In a short-circuit condition, there is no photo-induced current density or short-circuit current density (J_{SC}) generated by D2 as the device does not follow the photovoltaic operation. However, D1 with the ITO/PEDOT:PSS/P3HT:N2200 (1:1)/BCP/Al structure shows 0.28% maximum *PCE*, 41.0% fill factor (*FF*), 1.58 mA/cm^2 short-circuit current density (J_{SC}), and 0.43 V open circuit voltage (V_{OC}). Yoshida *et al*. investigated the *J–V* characteristics of the P3HT:N2200 BHJ photovoltaic with the ITO/ZnO/P3HT:N2200/MoO_3/Ag device structure [59]. They reported that the photovoltaic parameters are 0.196% maximum *PCE*, 48.95% *FF*, 0.66 mA/cm^2 short-circuit current density (J_{SC}), and 0.60 V open-circuit voltage (V_{OC}). A 0.82% maximum PCE with 3.5 mA/cm^2 J_{SC}, 0.45 V V_{OC}, and 0.52% *FF* were reported by Huajun Xu in a P3HT:N2200 dye-sensitized solar cell [60]. Shinzaburo *et al*. reported a 3 mA/cm^2 short-circuit current density (J_{SC}) of the P3HT:N2200 BHJ solar cell [53].

Conclusions

In this paper, we report the experimentally observed photoabsorption energies of P3HT, N2200, and small-gap fullerene-ethyl nipecotate using UV–vis absorption spectroscopy. The maximum photon absorbed by the P3HT polymer generates the maximum exciton. The experimental results from the UV–vis spectra were used to calculate the band-gap energy of the materials in the solution state. The band gaps of P3HT and N2200 obtained in this study are in good agreement with those in the literature [50, 52, 53]. The interfaces between P3HT and N2200 and between P3HT and small-gap fullerene-ethyl nipecotate are of great importance because of the exciton dissociation or charge separation that takes place in the interface area. The fabricated ITO/PEDOT:PSS/P3HT:Fullerene-EN (1:0.6)/LiF/Al BHJ structure with small-gap fullerene-ethyl nipecotate is not suitable for photovoltaic operations. With the P3HT:N2200 blend, the BHJ structure follows the photovoltaic characteristics with 1.58 mA/cm^2 short-circuit current density (J_{SC}).

Acknowledgments

The authors acknowledge *(i)* the Department of Chemistry, SUST for the access of using their laboratory facilities for UV–vis and PL measurements, *(ii)* the Central Instruments Facility and Organic Electronics Laboratory, IIT Guwahati, India for providing various instrumental facilities for organic solar cell device fabrication and characterizations, and *(iii)* Dr. Ishtiaque M. Syed Professor, Department of Physics, University of Dhaka and Dr. Mohammad Afsar Uddin from the University of Illinois at Urbana-Champaign for their helpful discussions.

References

[1] Rasmussen, S.C. 2018. 2000 Nobel Prize in Chemistry. Acetylene Polym. 125–132, https://doi.org/10.1007/978-3-319-95489-9_7.

[2] Chiang, C.K., Fincher Jr, C.R., Park, Y.W., Heeger, A.J., Shirakawa, H., Louis, E.J., Gau, S.C., MacDiarmid, A.G. 1977. Electrical conductivity in doped polyacetylene. Physi. Rev. Lett. 39(17): 1098, https://doi.org/10.1103/PhysRevLett.39.1098.

[3] Coropceanu, V., Cornil, J., Filho, D.A.d.S., Olivier, Y., Silbey, R., Bredas, J.-L. 2007. Charge Transport in Organic Semiconductors. Chem. Rev. 107(4): 926–952, https://doi.org/10.1021/cr050140x.

[4] Han, M.Y., Özyilmaz, B., Zhang, Y., Kim, P. 2007. Energy band-gap engineering of graphene nanoribbons. Phys. Rev. Lett. 98(20): 206805. https://doi.org/10.1103/PhysRevLett.98.206805.

[5] Brédas, J.L., Heeger, A.J. 1994. Influence of donor and acceptor substituents on the electronic characteristics of poly (paraphenylene vinylene) and poly (para phenylen). Chem. Phys. Lett. 217(5–6): 507–512, https://doi.org/10.1016/0009-2614(93)E1421-C.

[6] Zhao, W., Ye, L., Zhang, S., Yao, H., Sun, M., Hou, J. 2015. An easily accessible cathode buffer layer for achieving multiple high performance polymer photovoltaic cells. J. Phys. Chem. C. 119(49): 27322–27329, https://doi.org/10.1021/acs.jpcc.5b09575.

[7] Wang, W., Yuan, J., Shi, G., Zhu, X., Shi, S., Liu, Z., Han, L., Wang, H.Q., Ma, W. 2015. Inverted planar heterojunction perovskite solar cells

employing polymer as the electron conductor. ACS Appl. Mater. Interfaces. 7(7): 3994–3999, https://doi.org/10.1021/am506785k.

[8] Yuan, J., Ma, W. 2015. High efficiency all-polymer solar cells realized by the synergistic effect between the polymer side-chain structure and solvent additive. J. Mater. Chem. A. 3(13): 7077–7085, https://doi.org/10.1039/C4TA06648K.

[9] Liu, S.Y., Jung, J.W., Li, C.Z., Huang, J., Zhang, J., Chen, H., Jen, A.K.Y. 2015. Three-dimensional molecular donors combined with polymeric acceptors for high performance fullerene-free organic photovoltaic devices. J. Mater. Chem. A. 3(44): 22162–22169, https://doi.org/10.1039/C5TA06639E.

[10] Leal, L.A., de Sousa, L.E., de Brito, P.P., Neto, B.G.E., Ceschin, A.M., da Cunha, W.F., Ribeiro, L.A., Silva Filho, D.A.D. 2018. Optical properties of P3HT and N2200 polymers: a performance study of an optimally tuned DFT functional. J. Mol. Model. 24(1): 1–11, https://doi.org/10.1007/s00894-017-3542-2.

[11] Liu, Q., Jiang, Y., Jin, K., Qin, J., Xu, J., Li, W., Xiong, J., Liu, J., Xiao, Z., Sun, K., Yang, S. 2020. 18% Efficiency organic solar cells. Sci. Bull. 65(4): 272–275, https://doi.org/10.1016/j.scib.2020.01.001.

[12] Sun, H., Liu, T., Yu, J., Lau, T.K., Zhang, G., Zhang, Y., Su, M., Tang, Y., Ma, R., Liu, B., Liang, J. 2019. A monothiophene unit incorporating both fluoro and ester substitution enabling high-performance donor polymers for non-fullerene solar cells with 16.4% efficiency. Energy Environ. Sci. 12(11): 3328–3337, https://doi.org/10.1039/C9EE01890E.

[13] Tajima, M., Iwai, T., Toyota, H., Binetti, S., Macdonald, D. 2010. Fine structure due to donor–acceptor pair luminescence in compensated Si. Appl. Phys. Expr. 3(7): 071301, https://doi.org/10.1143/APEX.3.071301.

[14] Noguchi, Y., Saeki, A., Fujiwara, T., Yamanaka, S., Kumano, M., Sakurai, T., Matsuyama, N., Nakano, M., Hirao, N., Ohishi, Y., Seki, S. 2015. Pressure modulation of backbone conformation and intermolecular distance of conjugated polymers toward understanding the dynamism of π-figuration of their conjugated system. J. Phys. Chem. B. 119(24): 7219–7230, https://doi.org/10.1021/jp5100389.

[15] Yu, G., Zhang, C., Heeger, A.J. 1994. Dual-function semiconducting polymer devices: Light-emitting and photodetecting diodes. Appl. Phys. Lett. 64(12): 1540–1542, https://doi.org/10.1063/1.111885.

[16] Sariciftci, N.S. 1999. Polymeric photovoltaic materials. Curr. Opin. Solid State Mater. Sci. 4(4): 373–378, https://doi.org/10.1016/S1359-0286(99)00044-3.

[17] Antoniadis, H. 1993. Photovoltaic effects at polymer/metal interface. Polym. Preprints. 34(2): 490.

[18] Li, S., Liu, W., Li, C.Z., Shi, M., Chen, H. 2017. Efficient organic solar cells with non-fullerene acceptors. Small. 13(37): 1701120, https://doi.org/10.1002/smll.201701120.

[19] Barr, M.G., Chambon, S., Fahy, A., Jones, T.W., Marcus, M.A., Kilcoyne, A.D., Dastoor, P.C., Griffith, M.J.. Holmes, N.P. 2021. Nanomorphology of eco-friendly colloidal inks, relating non-fullerene acceptor surface energy to structure formation. Mater. Chem. Front. 5(5): 2218–2233, https://doi.org/10.1039/D0QM00980F.

[20] Yu, G., Gao, J., Hummelen, J.C., Wudl, F., Heeger, A.J. 1995. Polymer photovoltaic cells: enhanced efficiencies via a network of internal donor-acceptor heterojunctions. Science. 270(5243): 1789–1791, https://doi.org/10.1126/science.270.5243.1789.

[21] Xiong, Y., Ye, L., Zhang, C. 2022. Eco-friendly solution processing of all-polymer solar cells: Recent advances and future perspective. J. Polym. Sci. 60(6): 945–960, https://doi.org/10.1002/pol.20210745.

[22] Sun, R., Wang, W., Yu, H., Chen, Z., Xia, X., Shen, H., Guo, J., Shi, M., Zheng, Y., Wu, Y., Yang, W. 2021. Achieving over 17% efficiency of ternary all-polymer solar cells with two well-compatible polymer acceptors. Joule. 5(6): 1548–1565, https://doi.org/10.1016/j.joule.2021.04.007.

[23] Bi, P., Zhang, S., Chen, Z., Xu, Y., Cui, Y., Zhang, T., Ren, J., Qin, J., Hong, L., Hao, X., Hou, J. 2021. Reduced non-radiative charge recombination enables organic photovoltaic cell approaching 19% efficiency. Joule. 5(9): 2408–2419, https://doi.org/10.1016/j.joule.2021.06.020.

[24] Xiong, J., Xu, J., Jiang, Y., Xiao, Z., Bao, Q., Hao, F., Feng, Y., Zhang, B., Jin, Z., Ding, L. 2020. Fused-ring bislactone building blocks for polymer donors. Sci. Bull. 65: 1792, https://doi.org/10.1016/j.scib.2020.07.018.

[25] Zhan, L., Li, S., Xia, X., Li, Y., Lu, X., Zuo, L., Shi, M., Chen, H. 2021. Layer-by-layer processed ternary organic photovoltaics with efficiency over 18%. Adv. Mater. 33(12): 2007231, https://doi.org/10.1002/adma.202007231.

[26] Cui, Y., Xu, Y., Yao, H., Bi, P., Hong, L., Zhang, J., Zu, Y., Zhang, T., Qin, J., Ren, J., Chen, Z. 2021. Single-junction organic photovoltaic cell with 19% efficiency. Adv. Mater. 33(41): 2102420, https://doi.org/10.1002/adma.202102420.

[27] Wong, W.Y., Wang, X.Z., He, Z., Djurišić, A.B., Yip, C.T., Cheung, K.Y., Wang, H., Mak, C.S., Chan, W.K. 2011. Metallated conjugated polymers as a new avenue towards high-efficiency polymer solar cells. Mater. Sustain. Energy. 51–57, https://doi.org/10.1142/9789814317665_0007.

[28] Pandey, R., Holmes, R.J. 2010. Graded Donor-Acceptor Heterojunctions for Efficient Organic Photovoltaic Cells. Adv. Mater. 22(46): 5301–5305, https://doi.org/10.1002/adma.201002454.

[29] Hoven, C.V., Dang, X.D., Coffin, R.C., Peet, J., Nguyen, T.Q., Bazan, G.C. 2010. Improved performance of polymer bulk heterojunction solar cells through the reduction of phase separation via solvent additives. Adv. Mater. 22(8): E63–E66, https://doi.org/10.1002/adma.200903677.

[30] Singh, A., Dey, A., Das, D., Iyer, P.K. 2016. Effect of dual cathode buffer layer on the charge carrier dynamics of rrP3HT: PCBM based bulk heterojunction solar cell. ACS Appl. Mater. Interfaces. 8(17): 10904–10910, https://doi.org/10.1021/acsami.6b03102.

[31] Brabec, C.J., Shaheen, S.E., Winder, C., Sariciftci, N.S., Denk, P. 2002. Effect of LiF/metal electrodes on the performance of plastic solar cells. Appl. Phys. Lett. 80(7): 1288–1290, https://doi.org/10.1063/1.1446988.

[32] Roy, J.K., Kar, S., Leszczynski, J. 2019. Optoelectronic properties of c60 and c70 fullerene derivatives: Designing and evaluating novel candidates for efficient p3ht polymer solar cells. Materials. 12(14): 2282, https://doi.org/10.3390/ma12142282.

[33] Shrotriya, V., Ouyang, J., Tseng, R.J., Li, G., Yang, Y. 2005. Absorption spectra modification in poly (3-hexylthiophene): methanofullerene blend thin films. Chem. Phys. Lett. 411(1–3): 138–143, https://doi.org/10.1016/j.cplett.2005.06.027.

[34] Yin, B., Yang, L., Liu, Y., Chen, Y., Qi, Q., Zhang, F., Yin, S. 2010. Solution-processed bulk heterojunction organic solar cells based on an oligothiophene derivative. Appl. Phys. Lett. 97(2): 139, https://doi.org/10.1063/1.3460911.

[35] Li, G., Shrotriya, V., Yao, Y., Huang, J., Yang, Y. 2007. Manipulating regioregular poly (3-hexylthiophene):[6, 6]-phenyl-C 61-butyric acid methyl ester blends—route towards high efficiency polymer solar cells. J. Mater. Chem. 17(30): 3126–3140, https://doi.org/10.1039/B703075B.

[36] Geng, J., Kong, B.S., Yang, S.B., Youn, S.C., Park, S., Joo, T., Jung, H.T. 2008. Effect of SWNT defects on the electron transfer properties in P3HT/SWNT hybrid materials. Adv. Funct. Mater. 18(18): 2659–2665, https://doi.org/10.1002/adfm.200800496.

[37] Wen, G., Zou, X., Hu, R., Peng, J., Chen, Z., He, X., Dong, G., Zhang, W. 2021. Ground-and excited-state characteristics in photovoltaic polymer N2200. RSC Adv. 11(33): 20191–20199, https://doi.org/10.1039/D1RA01474A.

[38] Zhang, Q., Chen, Z., Ma, W., Xie, Z., Han, Y. 2019. Optimizing domain size and phase purity in all-polymer solar cells by solution ordered aggregation and confinement effect of the acceptor. J. Mater. Chem. C. 7(40): 1256–12571, https://doi.org/10.1039/C9TC03697K.

[39] Chen, T.A., Wu, X., Rieke, R.D. 1995. Regiocontrolled synthesis of poly (3-alkylthiophenes) mediated by Rieke zinc: their characterization and solid-state properties. J. Am. Chem. Soc. 117(1): 233–244, https://doi.org/10.1021/ja00106a027.

[40] Kasha, M. 1950. Characterization of electronic transitions in complex molecules. Discuss. Faraday Soc. 9: 14–19, https://doi.org/10.1039/DF9500900014.

[41] McNaught, A.D., *et al*. 1997. Compendium of chemical terminology. Oxford: Blackwell Science, 1669.

[42] Tanveer, M., Habib, A., Khan, M.B. 2015. Structural and optical properties of electrospun ZnO nanofibres applied to P3HT: PCBM organic photovoltaic devices. J. Exp. Nanosci. 10(8): 640–650, https://doi.org/10.1080/17458080.2013.869841.

[43] Tiffour, I., Dehbi, A., Mourad, A.H.I., Belfedal, A. 2016. Synthesis and characterization of a new organic semiconductor material. Mater. Chem. Phys. 178: 49–56, https://doi.org/10.1016/j.matchemphys.2016.04.054.

[44] Tauc, J. 1968. Optical properties and electronic structure of amorphous Ge and Si. Mater. Res. Bull. 3(1): 37–46, https://doi.org/10.1016/0025-5408(68)90023-8.

[45] Stenzel, O. 2015. The physics of thin film optical spectra. Germany: Springer.

[46] Davis, E.A., Mott, N. 1970. Conduction in non-crystalline systems V. Conductivity, optical absorption and photoconductivity in amorphous semiconductors. Philos. Mag. 22(179): 0903–0922, https://doi.org/10.1080/14786437008221061.

[47] Johannes, A.Z., Pingak, R.K., Bukit, M. 2020. Tauc Plot Software: Calculating energy gap values of organic materials based on Ultraviolet-Visible absorbance spectrum. IOP Conf. Ser. Mater. Sci. Eng. 823(1): 012030, http://dx.doi.org/10.1088/1757-899X/823/1/012030.

[48] Jubu, P.R., Yam, F.K., Igba, V.M., Beh, K.P. 2020. Tauc-plot scale and extrapolation effect on bandgap estimation from UV–vis–NIR data–a case study of β-Ga2O3. J. Solid State Chem. 290: 121576, https://doi.org/10.1016/j.jssc.2020.121576.

[49] Prasad, S.S., Divya, G., Kumar, K.S. 2021. September. P3HT Thin Films And Their Optical Characterization. Int. Conf. Adv. Comput. Commun. Embed. Secur. Syst. 5–8, https://doi.org/10.1109/ACCESS51619.2021.9563335.

[50] Anefnaf, I., Benhaddou, N., Aazou, S., Abd-Lefdil, M., Sekkat, Z. 2016. November. Optical, structural and Photoconductivity properties of organic photovoltaic thin films based on polymer/fullerene. Int. Renew. Sustain. Energy Conf. 801–804, https://doi.org/10.1109/IRSEC.2016.7983996.

[51] Guo, Y., Xia, D., Liu, B., Wu, H., Li, C., Tang, Z., Xiao, C., Li, W. 2019. Small band gap boron dipyrromethene-based conjugated polymers for all-polymer solar cells: The effect of methyl units.

Macromolecules. 52(21): 8367–8373, https://doi.org/10.1021/acs.macromol.9b01525.
[52] Park, S.H., Kim, Y., Kwon, N.Y., Lee, Y.W., Woo, H.Y., Chae, W.S., Park, S., Cho, M.J., Choi, D.H. 2020. Significantly improved morphology and efficiency of nonhalogenated solvent-processed solar cells derived from a conjugated donor–acceptor block copolymer. Adv. Sci. 7(4): 1902470, https://doi.org/10.1002/advs.201902470.
[53] Ito, S., Hirata, T., Mori, D., Benten, H., Lee, L.T., Ohkita, H. 2013. Development of polymer blend solar cells composed of conjugated donor and acceptor polymers. J. Photopolym. Sci. Technol. 26(2): 175–180, https://doi.org/10.2494/photopolymer.26.175.
[54] Kumar, A., Sista, S., Yang, Y. 2009. Dipole induced anomalous S-shape I-V curves in polymer solar cells. J. Appl. Phys. 105(9): 094512, https://doi.org/10.1063/1.3117513.
[55] Oliveira, E.F., Lavarda, F.C. 2014. Molecular design of new P3HT derivatives: adjusting electronic energy levels for blends with PCBM. Mater. Chem. Phys. 148(3): 923–932, https://doi.org/10.1016/j.matchemphys.2014.09.002.
[56] Narayan, M.R., Singh, J. 2013. Study of the mechanism and rate of exciton dissociation at the donor-acceptor interface in bulk-heterojunction organic solar cells. J. Appl. Phys. 114(7): 073510, https://doi.org/10.1063/1.4818813.
[57] Gurney, R.S., Lidzey, D.G., Wang, T. 2019. A review of non-fullerene polymer solar cells: from device physics to morphology control. Rep. Prog. Phys. 82(3): 036601, http://dx.doi.org/10.1088/1361-6633/ab0530.
[58] Li, Y. 2012. Molecular design of photovoltaic materials for polymer solar cells: toward suitable electronic energy levels and broad absorption. Accounts Chem. Res. 45(5): 723–733, https://doi.org/10.1021/ar2002446.
[59] Yoshida, K., Chang, J.F., Chueh, C.C., Higashihara, T. 2021. Thiol-end-functionalized regioregular poly (3-hexylthiophene) for PbS quantum dot dispersions. ACS Appl. Polym. Mater. 3(9): 4450–4459, https://doi.org/10.1021/acsapm.1c 00436.
[60] Xu, H., Ohkita, H., Hirata, T., Benten, H., Ito, S. 2014. Near-IR dye sensitization of polymer blend solar cells. Polymer. 55(12): 2856–2860, https://doi.org/10.1016/j.polymer.2014.04.045.